Supporting Information

Light-Controlled Lipid Interaction and Membrane Organization in Photolipid Bilayer Vesicles

Patrick Urban†, Stefanie D. Pritzl†, David B. Konrad‡, James A. Frank‡, Carla Pernpeintner†,§, Christian R. Roeske†, Dirk Trauner‡,§,#,*, and Theobald Lohmüller†,§,*.

†Photonics and Optoelectronics Group, Department of Physics and CeNS, Ludwig-Maximilians-Universität München, Amalienstraße 54, 80799 Munich, Germany

‡Department of Chemistry and Center for Integrated Protein Science, Ludwig-Maximilians-Universität München, Butenandtstraße 5-13, 81377 Munich, Germany

#Department of Chemistry, New York University, Silver Center, 100 Washington Square East, Room 712, New York, 10003, United States

§Nanosystems Initiative Munich, Schellingstraße 4, 80799 Munich, Germany

1. Micropipette Aspiration

The working principle of micropipette aspiration[1] is shown below. Briefly, a vesicle is sucked into a micropipette. By controlling the pressure (Δp) and simultaneously recording the length (L_P) of the membrane tube, the area expansion modulus (K_A) and the bending modulus (k_c) can be calculated.

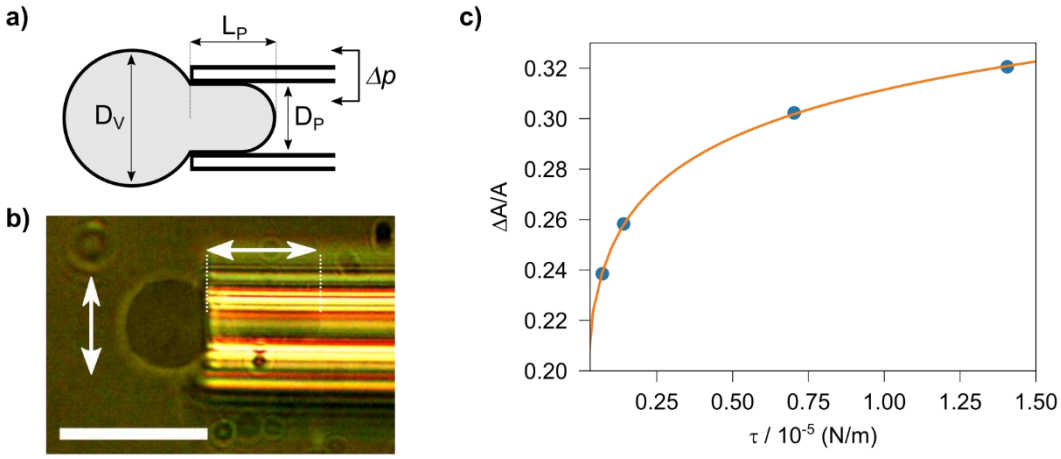

Figure S1: (a) Schematic illustration of the measured geometrical parameters D_V (vesicle diameter) and L_P (aspiration length). (b) Phase-contrast image of an aspirated vesicle (scale bar = 20 µm). (c) Experimental evaluation of the vesicle surface area change $\Delta A/A$ versus the membrane tension τ. Data points (blue) and the fit (orange) are used to extract membrane expansion and bending modulus.

The surface area change of the vesicle ΔA and the membrane tension τ can be extracted from the experiment according to:

$$\Delta A \approx \pi D_P \left(1 - \frac{D_P}{D_V}\right) L_P \quad \text{and}$$

$$\tau = \frac{D_P}{4\left(1 - \frac{D_P}{D_V}\right)} \Delta p$$

with D_P and D_V being the diameter of the pipette and the vesicle, Δp being the applied pressure and L_P the length of the membrane tube in the pipette (Figure S1).

The shape of the vesicle is linked to mechanical parameters according to

$$\frac{\Delta A}{A} = \frac{k_b T}{8\pi k_c} \ln\left(1 + \frac{\tau A}{\pi^2 k_c}\right) + \frac{\tau}{K_A}$$

with A being the vesicle surface area and ΔA the change induced by the tension τ

The first part of this sum describes the expansion due to smoothing out thermal shape fluctuations[2], which is relevant for the low tension regime. For high tensions, the undulations are fully smoothed and the direct expansion (only dependent on K_A) dominates.

The measurements were carried out on a microscope in phase contrast configuration (Axio Scope.A1, Zeiss) using a 100x water immersion objective (Achroplan 100x, W 1.00 NA, Ph3, Zeiss). Images were taken with a CMOS camera (EOS 550D, Canon). The micropipettes (Hilgenberg GmbH) were operated with a manual micropositioner. Two liquid filled reservoirs were used to control the pressure inside the pipette. The pressure was monitored using a pressure transducer (DP15, Validyne Inc.). The entire setup was built on top of a platform, which actively suppresses vibrations (Halcyonics_i4, Accuron).

2. Vibronic progression

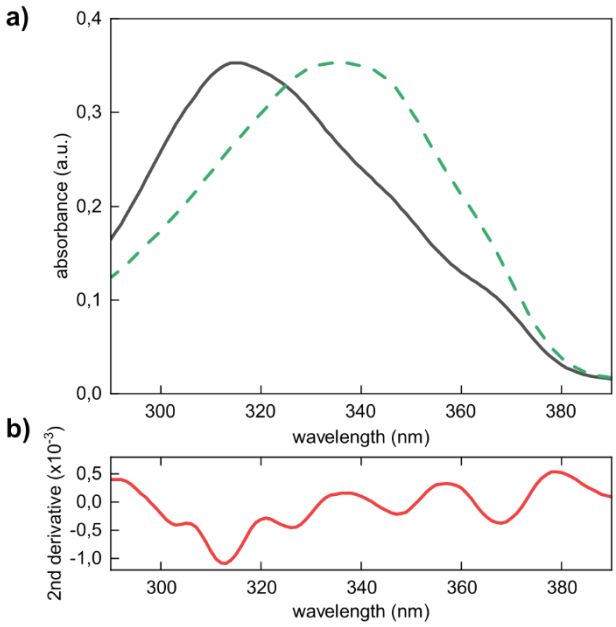

Figure S2: (a) Absorption spectrum of *azo*-**PC** SUVs (black). The vibrational states are visible between 320 nm and 380 nm. As comparison, the spectrum of *azo*-**PC** in $CHCl_3$ is also shown (green, dashed) (b) The second derivative of the absorbance spectrum of the SUVs shows the vibrational pattern. To reduce noise, a Savitzky-Golay filter was applied to the original spectrum before differentiation.

3. Estimation of the isomerization time

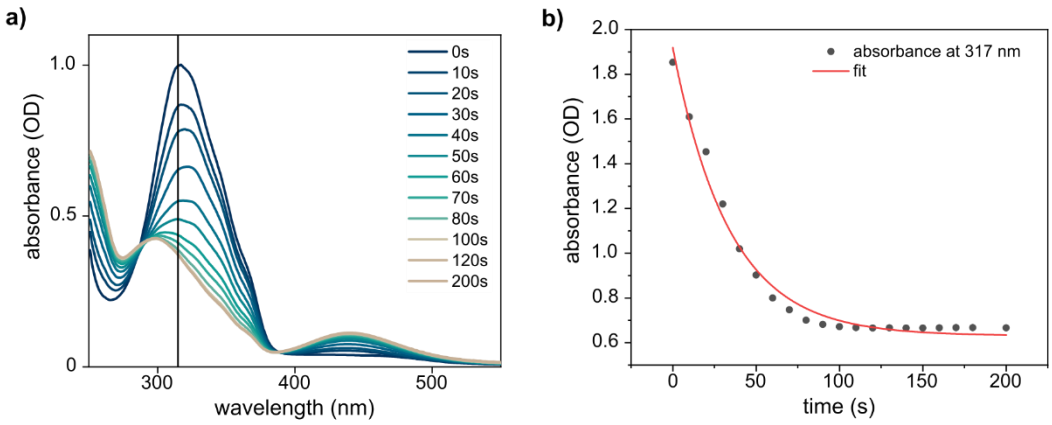

Figure S3: (a) Absorbance spectra of *azo*-**PC** SUVs under different illumination times with UV-A light (365 nm). The light source is placed 2 cm above the sample. The time specified in the legend indicates the total illumination duration. At t = 0s, the sample is in thermal equilibrium. (b) An exponential decay is fit to the absorbance values at 317 nm. For this illumination condition, the time constant for the isomerization process is 34±2 s.

4. Absorption spectra of SUVs with various mixtures of *azo*-PC and DPhPC

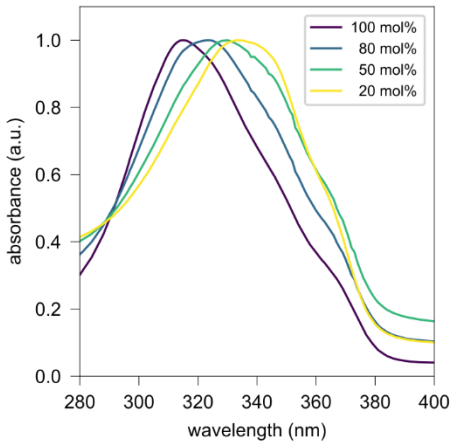

Figure S4: The legend indicates the concentration of *azo*-**PC**. The peak of the S0 → S2 transition shifts to higher wavelengths for decreasing *azo*-**PC** content.

5. Switching and Fusion of Domains

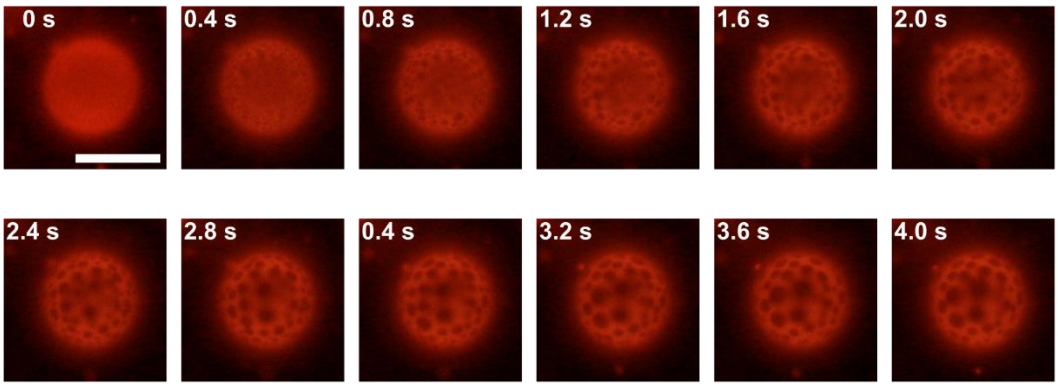

Figure S5: Switching of membrane domains in GUVs containing DPhPC, *azo*-**PC** and cholesterol (lipid ratio 4:4:2). After switching the photolipids from *cis* to *trans*, small membrane domains start to appear within a fraction of a second. The small domains merge into bigger domains until a photostationary state is reached. (Scale bar = 20µm)

Video V1: Domains of several vesicles are switched at the same time. The fluorescent filter set is indicated by the color of the frame. Green frames indicate the green filter set (U-MWG2, Olympus), grey frames indicate the UV filter set (U-MWU2, Olympus). The video is acquired with a color CMOS camera (EOS 5D Mark IV). The timespan between changing filters (~5 s) is cut to 1 s, to reduce the length of the movie. Otherwise, the movie is in real time.

6. Micropipette aspiration measurements of lipid mixtures

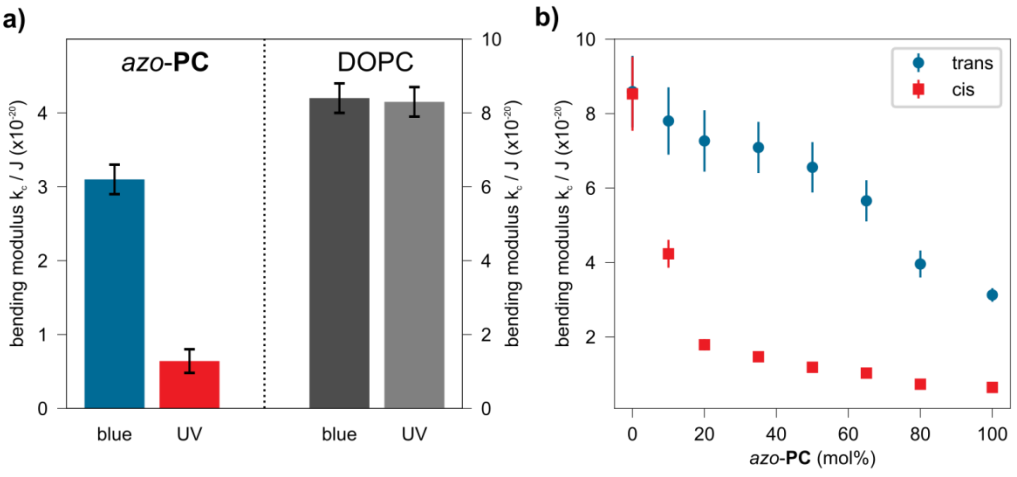

Figure S6: Mechanical properties of vesicles consisting of mixtures of *azo*-**PC** and DOPC. (a) For pure GUVs, DOPC has a higher bending rigidity than *azo*-**PC**. (b) Mixtures of *azo*-**PC** and DOPC exhibit a similar trend to mixtures of *azo*-**PC** and DPhPC.

7. Chemical synthesis and characterization

Equipment and Instruments

Nuclear magnetic resonance (NMR) spectroscopy: NMR spectra were acquired with the following spectrometers: Varian INOVA 400 (400 MHz for ^{1}H and 101 MHz for ^{13}C spectroscopy) and Bruker Avance III HD 400 with Cryo-head (400 MHz for ^{1}H and 101 MHz for ^{13}C spectroscopy). Chemical shifts (δ) are reported in parts per million (ppm) relative to tetramethylsilane (TMS). The deuterated solvents $CDCl_3$ and CD_3OD were used as internal references. Spin multiplicities are described as follows: s (singlet), d (doublet), t (triplet), q (quartet), quint (quintet), m (multiplet), br (broad) or a combination thereof. Structural analysis was conducted with ^{1}H- and ^{13}C-NMR spectra with the aid of additional 2D spectra (COSY, HMBC, HSQC, NOESY). Spectra analysis was conducted with the software MestReNova v.10.0.1-14719. The ^{31}P-NMR spectra were referenced using the ^{1}H-NMR spectra of the same compounds as an absolute reference.

Mass spectrometry (MS): The high resolution MS spectra were recorded on a Thermo Finnigan LTQ FT (ESI: electrospray ionization).

Infrared spectroscopy (IR): IR spectra were recorded on a *PerkinElmer* Spectrum BX II FT-IR device equipped with an attenuated total reflection (ATR) measuring unit. For measurements, the neat substances were directly applied as a thin film on the ATR unit. The measured wavenumbers are reported with their relative intensities which were classified as: vs (very strong), s (strong), m (medium), w (weak), vw (very weak), br (broad) or combinations thereof.

Methods

Unless otherwise noted, all reactions were magnetically stirred under inert gas (N_2) atmosphere using standard Schlenk techniques. Glassware was evacuated and dried by heating with a heat-gun (set to 550 °C). Drying over Na_2SO_4 implies stirring with an appropriate amount of anhydrous salt for several minutes followed by filtration through a glass frit and rinsing of the filter cake with additional solvent. Electric heating plates and oil baths were used for reactions at elevated temperature. For reactions below room temperature, the reaction vessel was cooled using a mixture of ice and water (0 °C). Stated reaction temperatures refer to the external bath temperature. Cannulas and syringes were used for the transfer of reagents or solvents which were flooded with inert gas (3×) before use. Purification by column chromatography was performed under elevated pressure (flash column chromatography) on Geduran© Si60 silica gel

(40-63 µm) from Merck KGaA. After flash column chromatography, the concentrated fractions were filtered once through a glass frit. Silica gel F_{254} TLC plates from Merck KGaA were used for monitoring reactions, analyzing fractions of column chromatography and measuring R_f values. To visualize the analytes, TLC plates were irradiated with UV light or appropriate staining solutions and subsequent heating. Freeze-drying refers to freezing of the respective sample in liquid nitrogen followed by evacuating the containing flask with high vacuum (< 1 mbar) and slow thawing to rt. Reaction yields refer to spectroscopically pure isolated amounts of compounds.

Chemicals

All chemicals were purchased from *Sigma Aldrich*, *Fisher Scientific*, *TCI Europe*, *Chempur*, *Alfa Aesar* or *Acros Organics*. Solvents purchased in technical grade quality were distilled under reduced pressure and used for purification procedures. Purchased solvents in HPLC and analytical grade quality were used without further purification. Unless otherwise noted, reactions were performed using dry solvents. Dichloromethane (CH_2Cl_2) and triethylamine (NEt_3) were dried by distillation from CaH_2. Other dry solvents were purchased from commercial sources (*Acros Organics*, *Fisher Scientific*) under inert gas atmosphere and over molecular sieves. All other reagents with a purity of >95% were purchased from commercial sources and used without further purification. For running extra dry reactions with synthetic compounds, stock solutions were prepared in PhMe, the respective amounts transferred into dried glassware and the solvent was removed by stirring under high vacuum (< 1 mbar). This procedure was followed by freeze-drying the compound to ensure that H_2O was fully removed. The CAM staining solution was prepared by dissolving ($Ce(NH_4)_2(NO_3)_6$ (0.5 g) and $(NH_4)_6Mo_7O_{24}$ $4H_2O$ (48 g) in H_2O (940 mL) and adding conc. H_2SO_4 (60 mL).

Experimental Procedures

*(R)-2-hydroxy-3-(stearoyloxy)propyl (2-(trimethylammonio)ethyl) phosphate (**lysoPC**)*

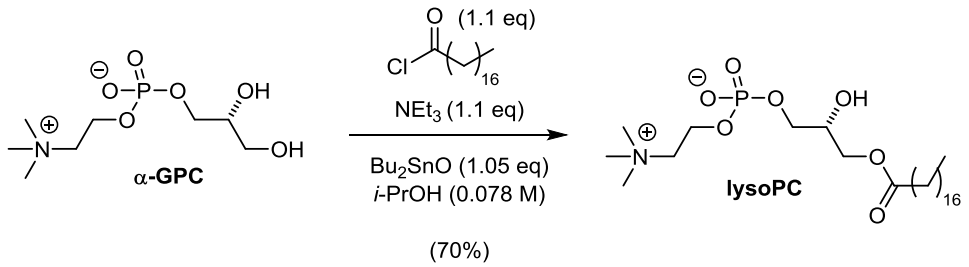

(*R*)-2,3-dihydroxypropyl (2-(trimethylammonio)ethyl) phosphate (**α-GPC**, 2.00 g, 7.78 mmol, 1.0 eq) and dibutyltin oxide (2.03 g, 8.16 mmol, 1.05 eq) were dissolved in *i*-PrOH (99.7 mL) and heated to 100 °C for 6 h 30 min. After cooling to 0 °C, NEt_3 (1.19 mL, 8.56 mmol, 1.1 eq) and stearoyl chloride (2.89 mL, 8.56 mmol, 1.1 eq) were added. The reaction was allowed to warm to rt and stirred for 16 h 30 min. Thereafter, the solvent was removed *in vacuo* and the residue directly purified by flash column chromatography (CH_2Cl_2:MeOH:H_2O = 9:1:0 → 10:4:0.5 → 10:8:2) to give (*R*)-2-hydroxy-3-(stearoyloxy)propyl (2-(trimethylammonio)ethyl) phosphate (**lysoPC**, 2.851 g, 5.444 mmol, 70%) as a white gum.

R_f (CH_2Cl_2:MeOH:H_2O = 10:4:0.5) = 0.19. (CAM)

^{1}H-NMR (400 MHz, CD_3OD) δ (ppm) = 4.33 – 4.25 (m, 2H), 4.18 (dd, *J* = 11.3, 4.5 Hz, 1H), 4.11 (dd, *J* = 11.4, 6.1 Hz, 1H), 4.03 – 3.93 (m, 1H), 3.93 – 3.85 (m, 2H), 3.68 – 3.62 (m, 2H), 3.23 (s, 9H), 2.36 (t, *J* = 7.5 Hz, 2H), 1.62 (quint, *J* = 7.1 Hz, 2H), 1.29 (s, 28H), 0.90 (t, *J* = 6.7 Hz, 3H).

^{13}C-NMR (101 MHz, CD_3OD) δ (ppm) = 175.4, 69.8 (d, *J* = 7.8 Hz), 67.4 (dt, *J* = 6.7, 3.1 Hz), 66.2, 60.4 (d, *J* = 5.0 Hz), 54.6 (t, *J* = 3.5 Hz), 34.9, 33.1, 30.8, 30.6, 30.5, 30.5, 30.2, 26.0, 23.8, 14.5.

HRMS (ESI): calc. for $C_{26}H_{55}NO_7P^+$ $[M + H^+]^+$: 524.3711, found: 524.3704.

IR (Diamond-ATR, neat) υ_{max} (cm^{-1}) = 3272 (br, w), 2916 (vs), 2850 (s), 1733 (m), 1467 (m), 1418 (vw), 1388 (vw), 1330 (vw), 1312 (vw), 1293 (w), 1273 (w), 1233, (s), 1215 (s), 1195

(m), 1176 (m), 1136 (m), 1985 (vs), 1053 (vs), 968 (s), 926 (m), 875 (w), 825 (m), 760 (m), 720 (s).

The analytical data is in accordance with the literature.[4]

*(R)-2-((4-(4-((4-butylphenyl)diazenyl)phenyl)butanoyl)oxy)-3-(stearoyloxy)propyl (2-(trimethylammonio)ethyl) phosphate (azo-**PC**) and (R)-3-((4-(4-((4-butylphenyl)diazenyl)phenyl)butanoyl)oxy)-2-(stearoyloxy)propyl (2-(trimethylammonio)ethyl) phosphate (iso-azo-**PC**)*

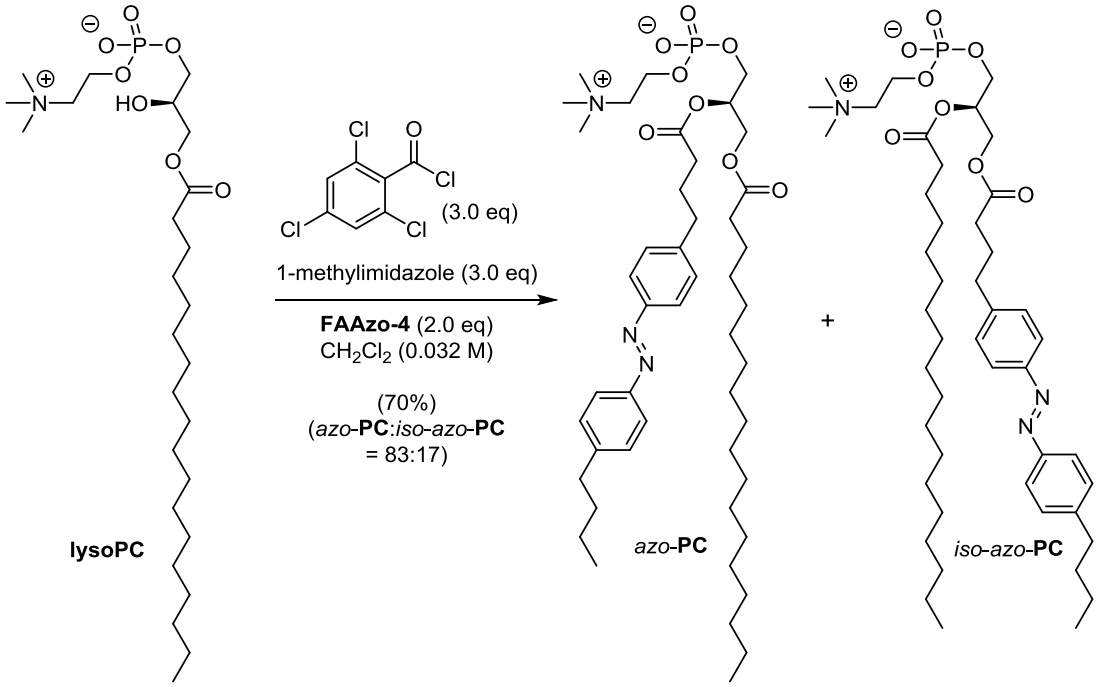

FAAzo-4[5] (614 mg, 1.91 mmol, 2.0 eq) was dissolved in CH_2Cl_2 (20 mL) and 1-methylimidazole (228 µL, 2.87 mmol, 3.0 eq) was added. The mixture was transferred to the secondary alcohol (**lysoPC**, 500 mg, 0.955 mmol, 1.0 eq) in CH_2Cl_2 (10 mL) and 2,4,6-trichlorobenzoyl chloride (410 µL, 2.87 mmol, 3.0 eq) was added dropwise. After stirring for 21 h at rt, the solution was directly subjected to purification via flash column chromatography (CH_2Cl_2:MeOH:H_2O = 1:0:0 → 99:1:0 → 95:5:0 → 8:2:0.1 → 7.5:2.5:0.1 → 7:3:0.2) to give a 83:17 mixture of (*R*)-2-((4-(4-((4-butylphenyl)diazenyl)phenyl)butanoyl)oxy)-3-(stearoyloxy)propyl (2-(trimethylammonio)ethyl) phosphate (*azo*-**PC**) and (*R*)-3-((4-(4-((4-butylphenyl)diazenyl)phenyl)butanoyl)oxy)-2-(stearoyloxy)propyl (2-

(trimethylammonio)ethyl) phosphate (*iso*-*azo*-**PC**) (555.3 mg, 0.6690 mmol, 70%) as an orange gum. These regioisomers could be separated using flash column chromatography (CH_2Cl_2:MeOH:conc. aq. NH_3 = 8:2:2%).

Note: Due to the photoswitching properties of the *azo*-**PC** and *iso*-*azo*-**PC** azobenzene moiety, the NMR spectra show a mixture of *cis*- and *trans*-isomers. The ^{1}H-NMR is reported for the thermodynamically more stable *trans*-isomer whereas a selection of diagnostic signals is reported for the ^{13}C-NMR.

Analytic data of *azo*-**PC**:

R_f (CH_2Cl_2:MeOH:H_2O = 10:4:0.5) = 0.41. (visible)

^{1}H NMR (400 MHz, $CDCl_3$) δ (ppm) = 7.80 (dd, *J* = 8.2, 2.2 Hz, 4H), 7.31 – 7.26 (m, 4H), 5.32 – 5.03 (m, 1H), 4.44 – 4.34 (m, 1H), 4.27 (s, 2H), 4.12 (dd, *J* = 12.2, 7.2 Hz, 1H), 3.98 – 3.86 (m, 2H), 3.75 (s, 2H), 3.31 (s, 9H), 2.76 – 2.59 (m, 4H), 2.39 – 2.29 (m, 2H), 2.29 – 2.17 (m, 2H), 2.01 – 1.88 (m, 2H), 1.62 (quint, *J* = 7.6 Hz, 2H), 1.56 – 1.46 (m, 2H), 1.35 (dt, *J* = 14.5, 7.3 Hz, 2H), 1.30 – 1.11 (m, 28H), 0.92 (t, *J* = 7.4 Hz, 3H), 0.85 (t, *J* = 6.7 Hz, 3H).

^{13}C NMR (101 MHz, $CDCl_3$) δ (ppm) = 173.7, 172.8, 151.3, 151.0, 146.4, 144.6, 129.2, 129.1, 122.9, 122.8, 70.8 (d, *J* = 7.5 Hz), 66.3 (d, *J* = 6.6 Hz), 63.5 (d, *J* = 4.4 Hz), 63.0, 59.4 (d, *J* = 4.5 Hz), 54.4, 35.7 34.9, 34.2, 33.6, 33.5, 32.0, 29.8, 29.8, 29.6, 29.5, 29.4, 29.3, 26.5, 25.0, 22.8, 22.4, 14.2, 14.0.

^{31}P NMR (162 MHz, $CDCl_3$) δ (ppm) = –1.08.

HRMS (ESI): calc. for $C_{46}H_{77}N_3O_8P^+$ $[M + H^+]^+$: 830.5443, found: 830.5440.

The analytical data is in accordance with the literature.[6]

Analytic data of *iso*-*azo*-**PC**:

R_f (CH_2Cl_2:MeOH:H_2O = 10:4:0.5) = 0.41. (visible)

^{1}H NMR (400 MHz, $CDCl_3$) δ (ppm) = 7.81 (d, *J* = 7.5 Hz, 4H), 7.30 (d, *J* = 7.9 Hz, 4H), 4.53 (s, 1H), 4.44 – 4.13 (m, 6H), 3.80 (s, 2H), 3.31 (s, 9H), 2.75 – 2.63 (m, 4H), 2.36 (t, *J* = 7.3 Hz, 2H), 2.28 (t, *J* = 7.5 Hz, 2H), 1.96 (quint, *J* = 7.5 Hz, 2H), 1.63 (quint, *J* = 7.7 Hz, 2H), 1.59 –

1.49 (m, 2H), 1.37 (dq, *J* = 14.6, 7.4 Hz, 2H), 1.23 (d, *J* = 5.0 Hz, 28H), 0.93 (t, *J* = 7.3 Hz, 3H), 0.87 (t, *J* = 6.7 Hz, 3H).

^{13}C NMR (101 MHz, $CDCl_3$) δ (ppm) = 173.5, 173.1, 151.2, 150.9, 146.4, 144.5, 129.2, 129.1, 122.9, 122.8, 70.9, 66.4, 66.3, 63.1, 62.7, 59.6, 54.5, 35.6, 34.9, 34.1, 33.5, 33.4, 31.9, 29.7, 29.7, 29.7, 29.6, 29.4, 29.2, 26.2, 24.9, 22.7, 22.4, 14.2, 14.0.

^{31}P NMR (162 MHz, $CDCl_3$) δ (ppm) = –2.17.

HRMS (ESI): calc. for $C_{46}H_{77}N_3O_8P^+$ $[M + H^+]^+$: 830.5443, found: 830.5439.

IR (Diamond-ATR, neat) υ_{max} (cm^{-1}) = 3250 (br, vw), 3028 (vw), 2957 (w), 2920 (vs), 2851 (s), 1734 (s), 1602 (w), 1580 (vw), 1495 (w), 1468 (m), 1416 (w), 1397, (w), 1378 (w), 1216 (s), 1180 (s), 1155 (s), 1085 (vs), 1057 (vs), 1012 (s), 968 (s), 928 (s), 874 (m), 838 (s), 799 (s), 722 (s).

NMR-Data

*(R)-2-hydroxy-3-(stearoyloxy)propyl (2-(trimethylammonio)ethyl) phosphate (**lysoPC**)*

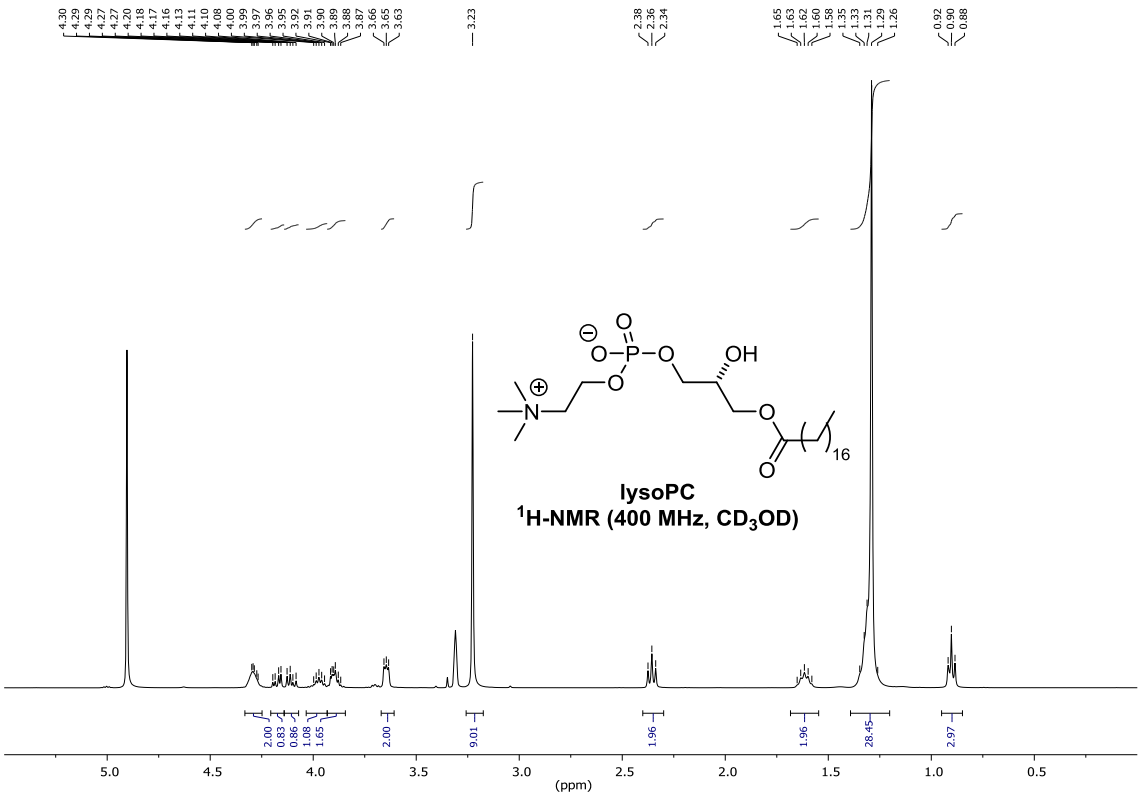

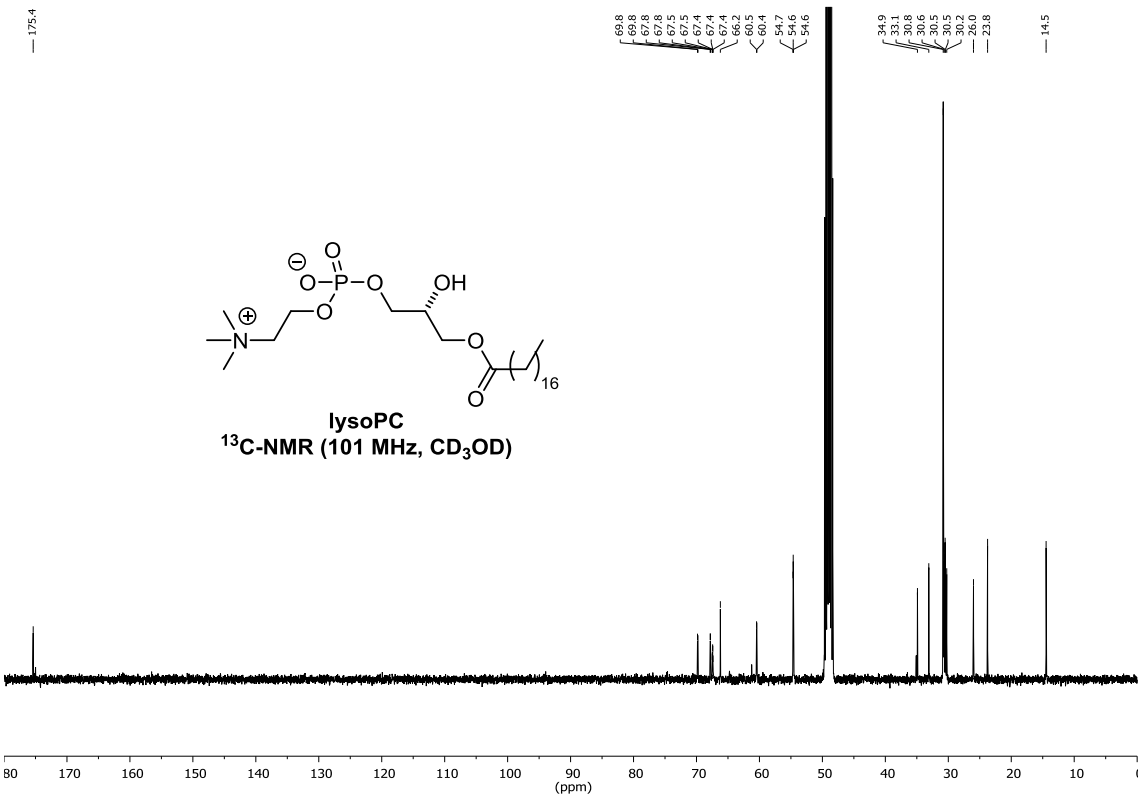

*(R)-2-((4-(4-((4-butylphenyl)diazenyl)phenyl)butanoyl)oxy)-3-(stearoyloxy)propyl (2-(trimethylammonio)ethyl) phosphate (azo-**PC**)*

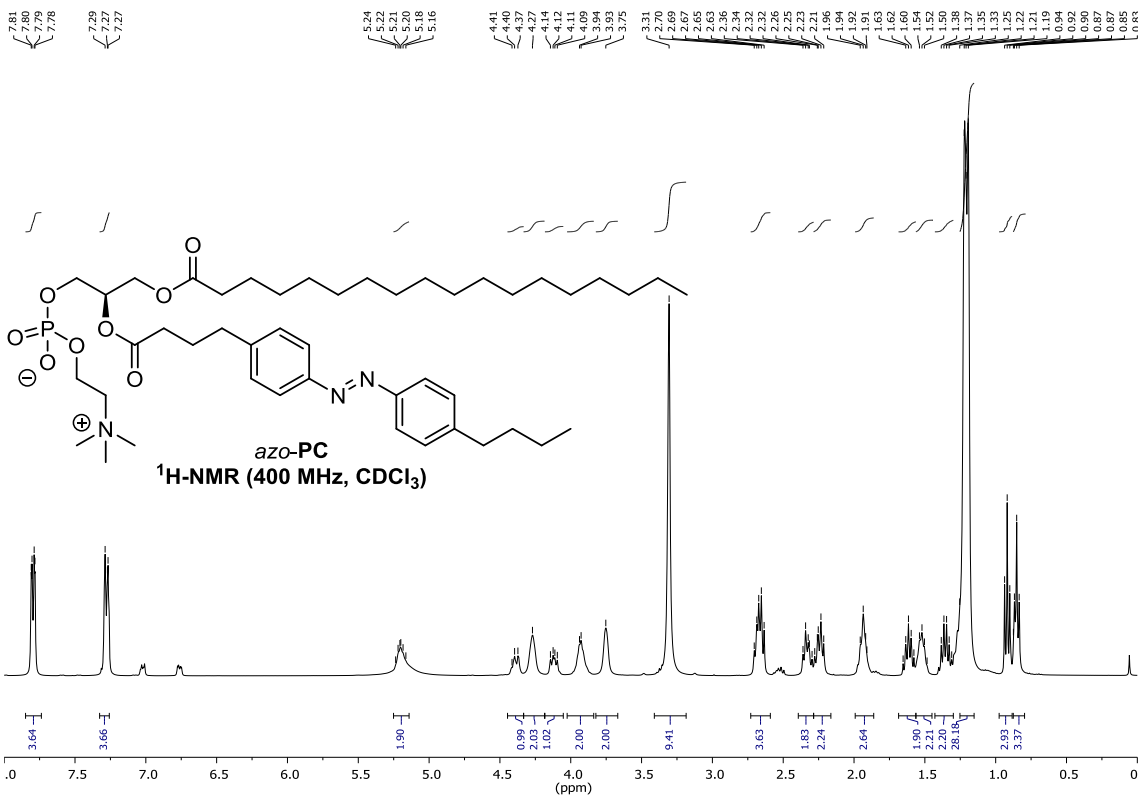

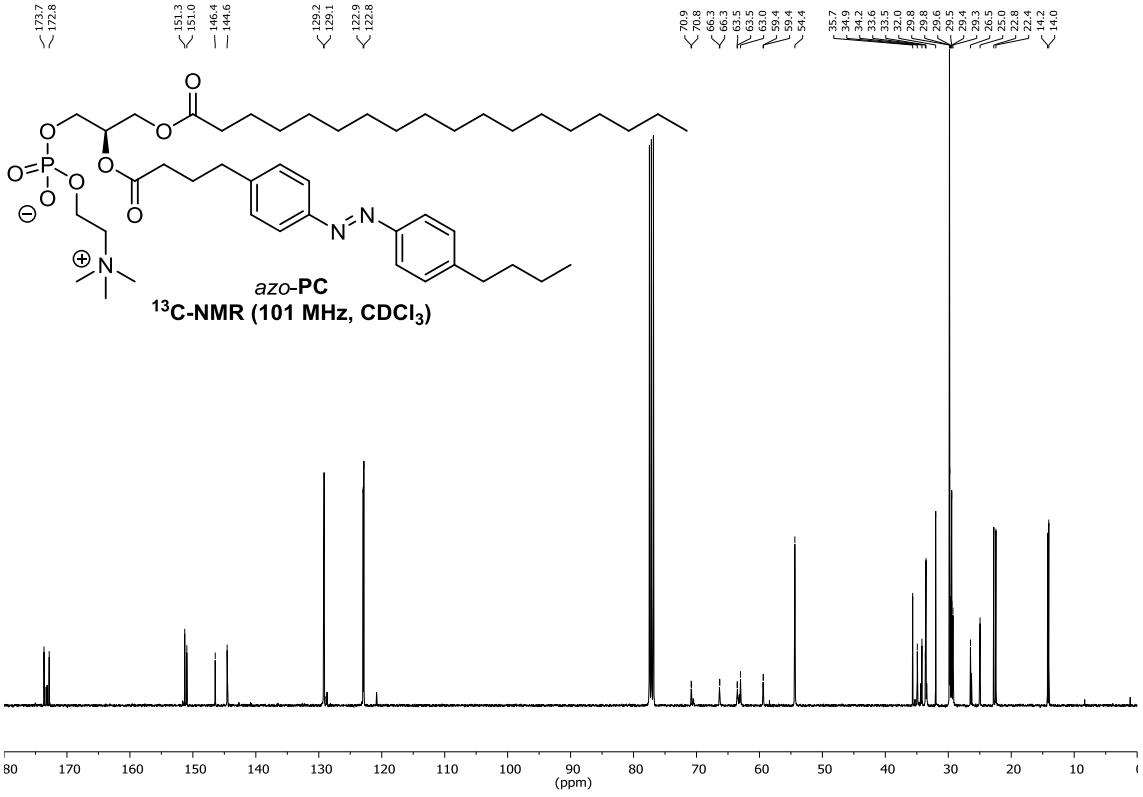

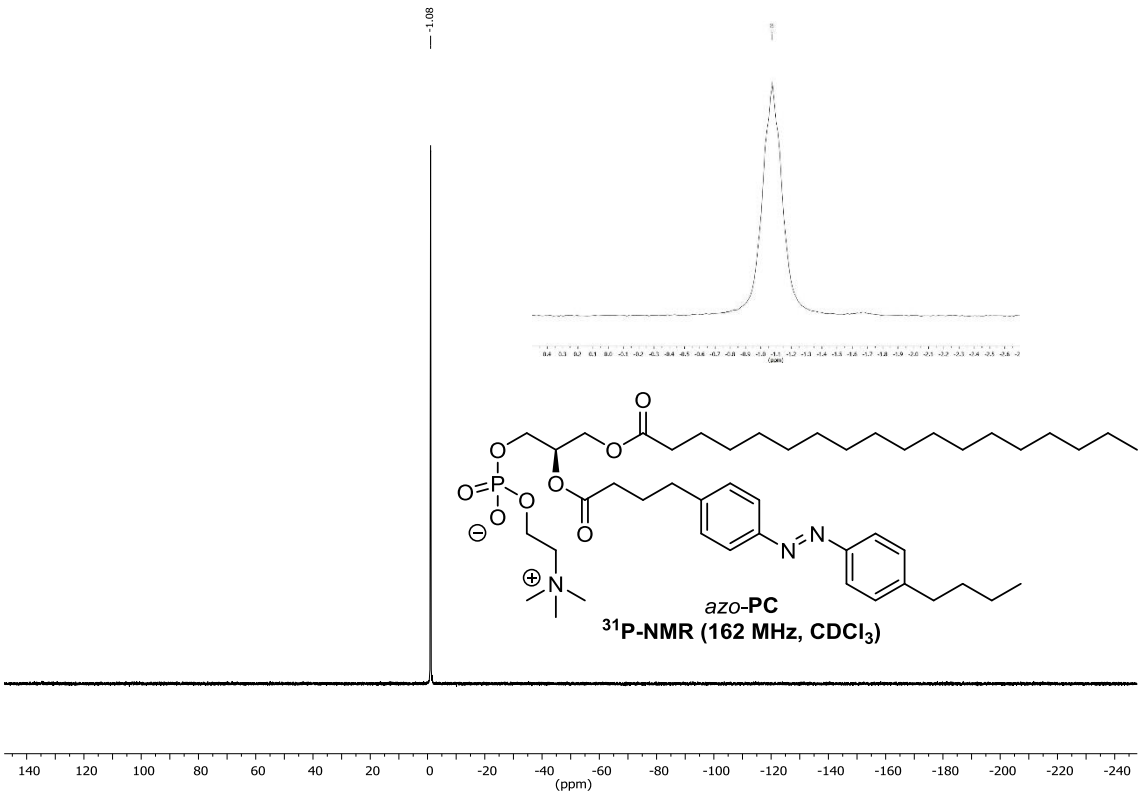

*(R)-3-((4-(4-((4-butylphenyl)diazenyl)phenyl)butanoyl)oxy)-2-(stearoyloxy)propyl (2-(trimethylammonio)ethyl) phosphate (iso-azo-**PC**)*

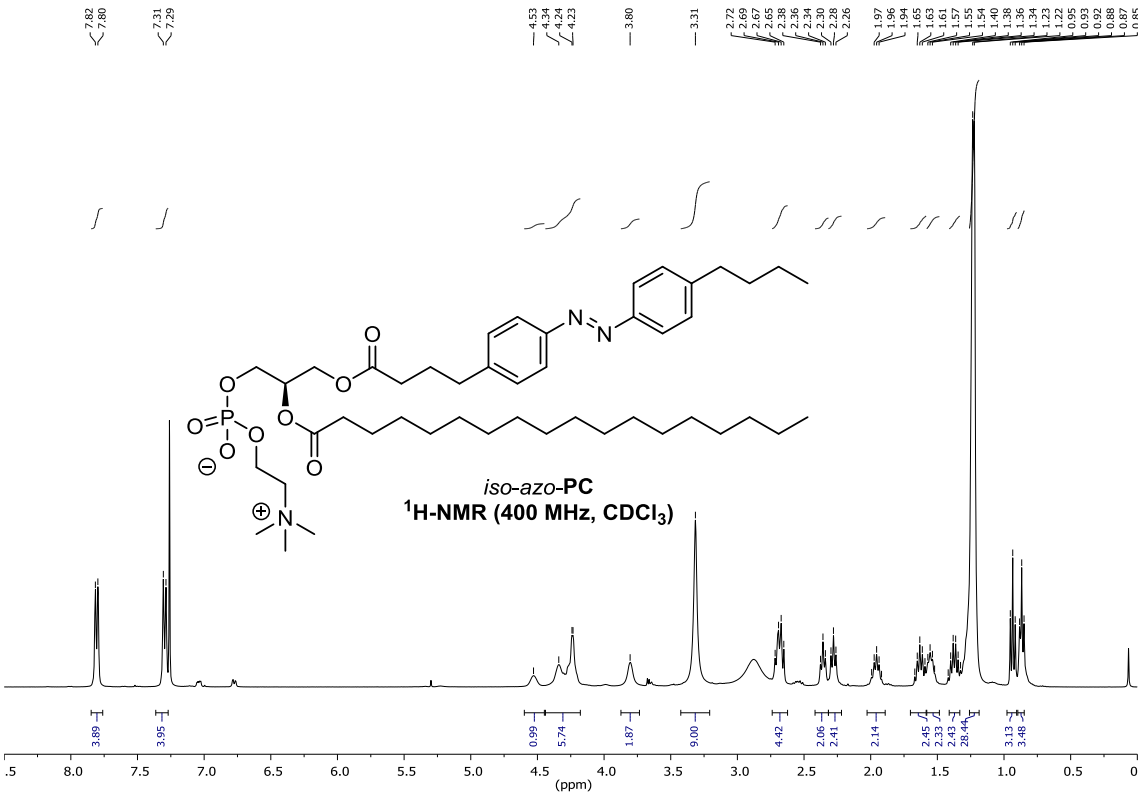

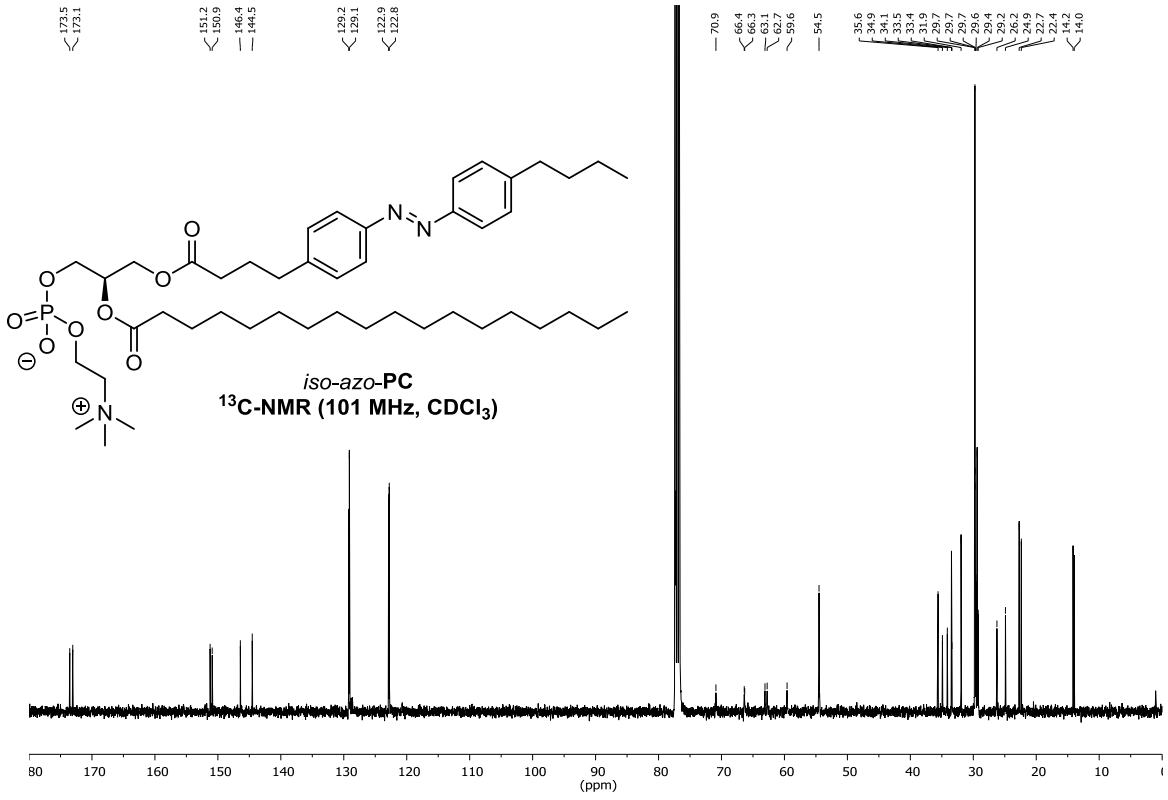
173.5
173.1
151.2
150.9
146.4
144.5
129.2
129.1
122.9
122.8
70.9
66.4
66.3
63.1
62.7
59.6
54.5
35.6
34.9
34.1
33.5
33.4
31.9
29.7
29.7
29.7
29.6
29.4
29.2
26.2
24.9
22.7
22.4
14.2
14.0
iso-azo-PC
13C-NMR (101 MHz, CDCl3)
(ppm)

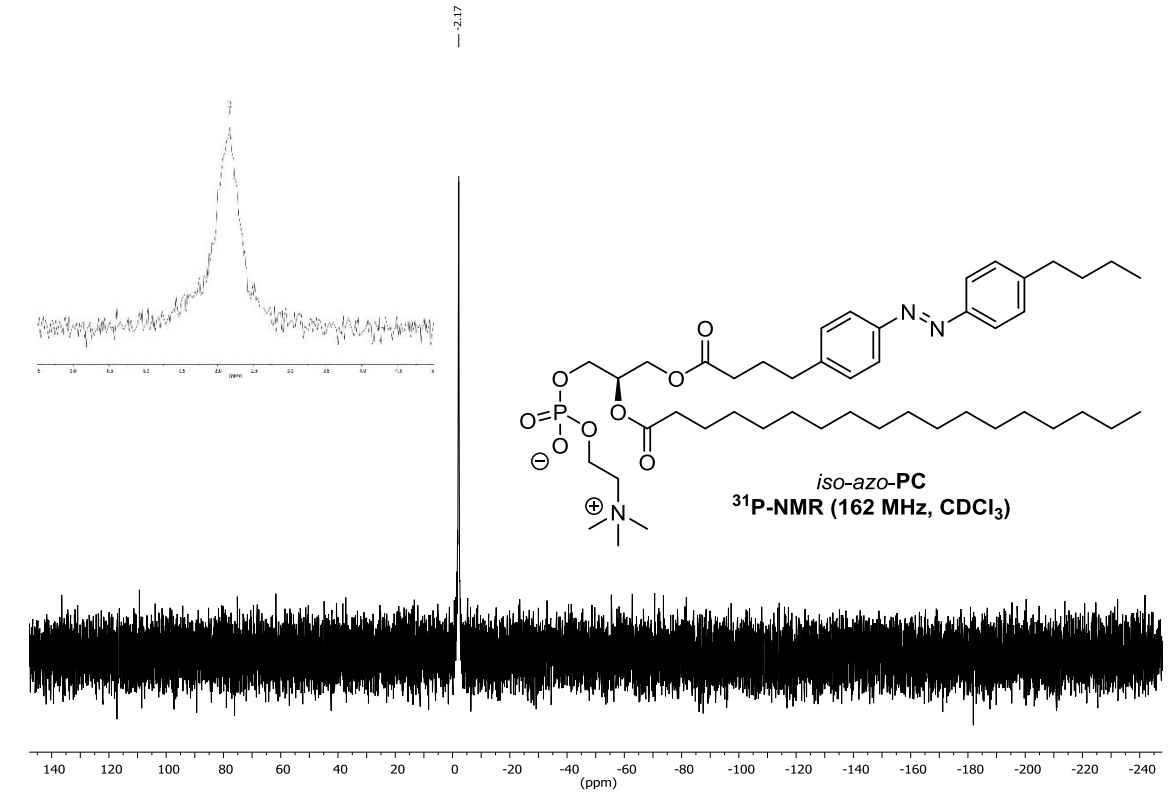
-2.17
iso-azo-PC
31P-NMR (162 MHz, CDCl3)
(ppm)

8. Supporting References

1. Kwok, R.; Evans, E., Thermoelasticity of large lecithin bilayer vesicles. *Biophys. J.* **1981,** *35* (3), 637-652.
2. Helfrich, W.; Servuss, R. M., Undulations, steric interaction and cohesion of fluid membranes. *Il Nuovo Cimento D* **1984,** *3* (1), 137-151.
3. Lin, W. C.; Yu, C. H.; Triffo, S.; Groves, J. T., Supported membrane formation, characterization, functionalization, and patterning for application in biological science and technology. *Curr. Protoc. Chem. Biol.* **2010,** *2* (4), 235-69.
4. Fasoli, E.; Arnone, A.; Caligiuri, A.; D'Arrigo, P.; de Ferra, L.; Servi, S., Tin-mediated synthesis of lyso-phospholipids. *Org. Biomol. Chem.* **2006,** *4* (15), 2974-2978.
5. Frank, J. A.; Moroni, M.; Moshourab, R.; Sumser, M.; Lewin, G. R.; Trauner, D., Photoswitchable fatty acids enable optical control of TRPV1. *Nat. Commun.* **2015,** *6*, 7118.
6. Pernpeintner, C.; Frank, J. A.; Urban, P.; Roeske, C. R.; Pritzl, S. D.; Trauner, D.; Lohmüller, T., Light-Controlled Membrane Mechanics and Shape Transitions of Photoswitchable Lipid Vesicles. *Langmuir* **2017,** *33* (16), 4083-4089.